Stoichiometry and specific assembly of Best ion channels

Shashank Bharill[a], Zhu Fu[a], Raz Palty[a], and Ehud Y. Isacoff[a,b,c,1]

[a]Department of Molecular and Cell Biology, and [b]Helen Wills Neuroscience Graduate Program, University of California, Berkeley, CA 94720; and [c]Physical Bioscience Division, Lawrence Berkeley National Laboratory, Berkeley, CA 94720

Edited* by Lily Yeh Jan, University of California, San Francisco, CA, and approved March 18, 2014 (received for review January 6, 2014)

Human Bestrophin 1 (hBest1) is a calcium-activated chloride channel that regulates neuronal excitability, synaptic activity, and retinal homeostasis. Mutations in hBest1 cause the autosomal-dominant Best macular dystrophy (BMD). Because hBest1 mutations cause BMD, but a knockout does not, we wondered if hBest1 mutants exert a dominant negative effect through interaction with other calcium-activated chloride channels, such as hBest2, 3, or 4, or transmembrane member 16A (TMEM16A), a member of another channel family. The subunit architecture of Best channels is debated, and their ability to form heteromeric channel assemblies is unclear. Using single-molecule subunit analysis, we find that each of hBest1, 2, 3, and 4 forms a homotetrameric channel. Despite considerable conservation among hBests, hBest1 has little or no interaction with other hBests or mTMEM16A. We identify the domain responsible for assembly specificity. This domain also plays a role in channel function. Our results indicate that Best channels preferentially self-assemble into homotetramers.

Bestrophin 1 is calcium-activated chloride channel (CACC) and has been shown to express in a variety of tissues (1). In the brain, Best1 plays a crucial role in the regulation of neuronal excitability and synaptic activity by releasing gliotransmitters such as glutamate and GABA from astrocytes upon G-protein–coupled receptor (GPCR) activation (2–5). In retinal pigment epithelium (RPE) cells, Best1 plays an important role in retinal homeostasis (1), and mutations in human Best1 have been implicated in several retinal degenerative diseases including Best Macular Dystrophy (BMD) (6–12) and Retinitis Pigmentosa (13).

The human bestrophin family includes three additional members; hBest2, 3, and 4 (14, 15). All four members function in heterologous cells (15–18) as anion-selective channels, whose main physiological charge carrier is chloride (15, 17, 19–22), but which also permeate glutamate and GABA (3, 4).

hBest1 contains six hydrophobic segments (S1–S6), with both N and C termini residing inside the cell. Two topology models have been proposed for hBest1 (15, 23). In the first model, S1, S2, S4, and S6 traverse the membrane, whereas S3 is intracellular and S5 forms a reentrant loop from outside (15). A more recent model has S1, S2, S5, and S6 traversing the membrane and S3 and S4, although hydrophobic, remaining on the intracellular side (23).

Best1 is activated by Ca^{2+} with a K_d of ~150 nM (24). Several pieces of evidence suggest that this activation is due to direct binding of Ca^{2+} (25, 26) to an EF hand located immediately after S6 (24). It is unclear how Ca^{2+}-binding gates the channel and whether the EF hand is part of the gate or communicates with it.

Although much progress has been made on Best channels (15, 17, 19–22, 27), several fundamental aspects of the structure and function of this channel family are not understood. First, previous biochemical analysis has indicated that Best1 is multimeric (22, 27) but led to conflicting assessments of the number of subunits in the channel, with experiments on human Best1 suggesting a tetramer or pentamer (22) but experiments on porcine Best1 suggesting a dimer (27). Second, although coimmunoprecipitation suggests that hBest1 interacts with hBest2 (22), it is unclear if this is direct interaction. Moreover, virtually nothing is known about the determinants of assembly.

In this study, we used single-molecule subunit counting and colocalization to address four major questions about the subunit assembly and function of hBest channels: (*i*) What is the subunit stoichiometry of hBest channels? (*ii*) Does hBest1 coassemble with any other member of the hBest family or with a member of different CACC family, transmembrane member 16A (TMEM16A)? (*iii*) How is subunit assembly specified? (*iv*) Does the assembly determinant play any role in channel function?

Results

Oligomeric Assembly of Bestrophins. Although earlier biochemical studies concluded that the Best1 channel is an oligomer, the estimate of the number of subunits ranged from 2 to 5 (22, 27). To resolve this question, we used the single-molecule subunit-counting method (28–33) to determine the number of subunits by counting the number of fluorescence-bleaching steps of monomeric enhanced green fluorescent protein (mEGFP)-tagged hBest1 in *Xenopus* oocytes [EGFP-tagged hBest1 was previously shown to be functional (34)]. The main advantages of this method are that: (*i*) the counting uses Total Internal Reflection Fluorescence Microscopy (TIRFM) to focus exclusively on functional channels in their native physiological environment, the plasma membrane of live cells, and (*ii*) because the level of expression can be easily controlled in oocytes, it is possible to obtain low enough densities so that each channel appears as an individual fluorescent spot that can be readily resolved from its neighbors.

Two differing topology models have been proposed for Best channels (15, 23). For simplicity, we numbered the domains according to the recent Milenkovic model (Fig. 1*A*), but we evaluate our results considering both the models.

The cDNA of hBest1, 2, 3, and 4 were tagged at either the N or C terminus with mEGFP (Fig. 1*A*) and transcribed in vitro, and the cRNA were injected into *Xenopus* oocytes (~1–2 ng per

Significance

Human Bestrophin (hBest) proteins represent a four-member family of calcium-activated chloride channels that regulate neuronal excitability, synaptic activity and retinal homeostasis. The number of subunits in a hBest channel and the ability to form heteromeric channels have been matters of debate. Using single molecule subunit analysis, we find that each of the hBest channels forms a homotetrameric channel. Despite considerable conservation among hBests, the members have little or no tendency to hetero-assemble. We identify the domain responsible for homo-assembly specificity.

Author contributions: S.B. and E.Y.I. designed research; S.B., Z.F., and R.P. performed research; Z.F. contributed new reagents/analytic tools; S.B. and R.P. analyzed data; and S.B. and E.Y.I. wrote the paper.

The authors declare no conflict of interest.

*This Direct Submission article had a prearranged editor.

[1]To whom correspondence should be addressed. E-mail: ehud@berkeley.edu.

This article contains supporting information online at www.pnas.org/lookup/suppl/doi:10.1073/pnas.1400248111/-/DCSupplemental.

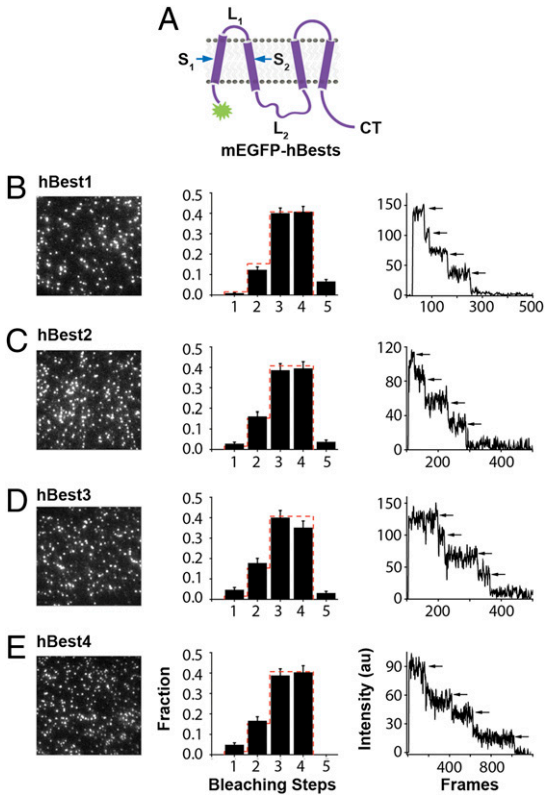

Fig. 1. Single-molecule subunit counting on the four members of the bestrophin family. (*A*) hBest cartoon here and elsewhere based on Milenkovic topology model. (*B–E*) Single-molecule irreversible photobleaching to count number of mEGFPs per fluorescent spot (i.e., number of subunits per channel) in hBest1 (*B*), hBest2 (*C*), hBest3 (*D*), and hBest4 (*E*). (*Left*) Images show first frame of the movie to indicate density of spots. (*Middle*) Average frequency distributions of number of bleaching steps (black bars) with error bars indicating SEM. Dashed red line indicates theoretical binominal distribution for tetramer with probability that mEGFP is fluorescent = 0.80. (*Right*) Fluorescence traces from single spots showing four steps of photobleaching.

cell). Following 1–2 d of expression, cells were devitelinized, illuminated in TIRFM, and imaged on a CCD camera at 10 frames per second (fps). Under constant illumination, the spots bleached to completion within 100 s. Bleaching steps were counted manually from 200 to 800 diffraction-limited spots from 5 to 10 optical patches taken from three to five oocytes from three to five different isolations. The average frequency distribution of the number of bleaching steps was plotted (Fig. 1*B*). The same analysis was performed on hBest2, 3, and 4 (Fig. 1 *C–E*). Each observed distribution was compared with predicted binomial distributions for cases in which the number of subunits was varied from two to five (*Materials and Methods*). The observed distribution for hBest1 was best accounted for by a binomial calculated for four subunits with a probability of 0.8 that mEGFP would be fluorescent (Fig. 1*B* and Figs. S1 and S2). This probability value of mEGFP being fluorescent is similar to what was observed previously for mEGFP fused to a number of other membrane proteins (28–33). Binomial predictions based on four subunits also accounted well for the other hBest family members (Fig. 1 *C–E*). These results show that each of the human bestrophin family members is a tetramer. To determine if bestrophins have the same tetrameric stoichiometry in mammalian cells, we tested hBest1 in HEK cells using a single-molecule pulldown (SiMPull) assay (35) (*Materials and Methods*). We observed a similar average frequency distribution of number of bleaching steps for Best1, confirming its tetrameric stoichiometry (Fig. S3).

Heteromeric Assembly Among Bestrophins. Because bestrophin 1 mutants have been shown to exert a dominant negative effect on wild-type bestrophin 1 (22, 36–38), and because hBest1 mutations cause BMD (39), but a knockout does not (40), we wondered if hBest1 mutants also exert a dominant negative effect through interaction with other CACCs, such as hBest2, 3, or 4, or TMEM16A, a member of another CACC family. To address this, we turned to the single-molecule colocalization method. Here too the TIRFM provides the advantage of determining the interaction between two functional channels on the surface of the live cell. To determine if hBest1 coassembles with one of the other hBests, we coexpressed mEGFP-tagged hBest1 with mCherry-tagged hBest2, 3, or 4. Similarly, to determine the coassembly between hBest1 and mTMEM16A, we used mCherry-tagged hBest1 and mEGFP-tagged mTMEM16A.

Coinjected oocytes were first illuminated at 590 nm to excite mCherry, and 200–300 frames were collected at 10 fps, following which 600–700 frames at 10 fps were collected under 488-nm illumination. Red frames were collected first so as to bleach mCherry and avoid any FRET between mEGFP and mCherry. The location of red and green spots was determined manually, and molecules located at the same spot in both red and green frames (within three pixels, 150 nm) were considered as colocalized (32, 33) (*Materials and Methods*). Chance (random) colocalization was calculated for each movie (28) (*Materials and Methods*) and subtracted to get the net colocalization values.

We first examined the degree of colocalization that would be detected between two completely unrelated tetrameric channels that should not coassemble (negative control) and between two tetrameric channels known to coassemble (positive control). For the negative control, we assessed colocalization between the mEGFP-tagged cyclic nucleotide-gated (CNG) ion channel, X-fa4 [which forms homotetrameric channels (32)], and mCherry-tagged hBest1. As expected, we observed a very small degree of colocalization of 2.9 ± 0.7% (Fig. 2*A*) above background (random colocalization) level. This negative control colocalization value was subtracted from the colocalization values of the test experiments, including the positive control. For the positive control, we coexpressed mEGFP-tagged hBest1 with mCherry-tagged hBest1 and observed 26.2 ± 1.7% colocalization between the green and red hBest1 subunits (Fig. 2*B*).

In contrast to the ∼26% colocalization of one hBest1 subunit with another hBest1, we observed ∼5- to 30-fold lower levels of colocalization (Student *t* test, $P < 0.01$) between mCherry-tagged hBest1 and mEGFP-tagged hBest2 (5.4 ± 1.5%), hBest3 (0.8 ± 1.2%), hBest4 (3.1 ± 0.8%), and mTMEM16A (1.1 ± 1.1%) (Fig. 2 *C–F*). These results indicate that hBest1 has a marked preference for interaction with itself over interaction with the other hBests or with mTMEM16A. To determine if the rest of the members in the bestrophin family follow the same trend as hBest1, we also checked colocalization among them. We observed significantly lower colocalization between hBest2–hBest3 (9.7 + 1.6%), hBest2–hBest4 (0.6 + 0.4%), and hBest3–hBest4 (1.9 + 0.6%) (Fig. S4) than between hBest1–hBest1 (26.2 + 1.7%) (Fig. 2*B*). Overall, this indicates that bestrophins have a marked preference for homomerization and seldom form heteromers.

To investigate further the preference of hBest1 for self-assembly, we counted bleaching steps of mEGFP–hBest1 coexpressed with an untagged version of either hBest1, 2, 3, or 4, or with untagged mTMEM16A. The rationale was that successful coassembly of untagged subunits with tagged ones would shift the observed distribution of spots with multiple fluorescent tags to lower values. As predicted, for mEGFP–hBest1 coexpressed with an untagged version of hBest1, we observed a substantial leftward shift in the frequency distribution (increased frequency of observation of 1 and 2 tags at the expense of 3 and 4 tags) compared to the binomial distribution for a tetramer with $P = 80\%$ (Figs. 1 and 3*A*). In contrast, little or no shift was seen for mEGFP–hBest1

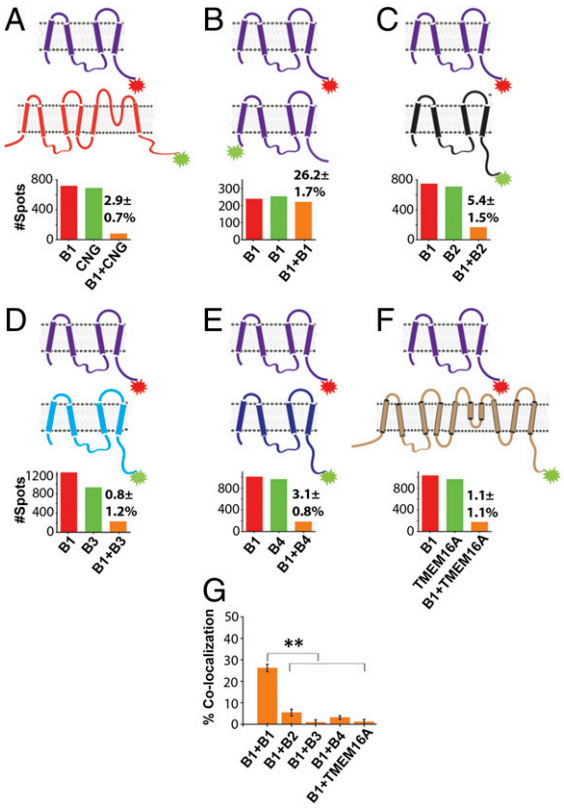

Fig. 2. Single-molecule colocalization analysis of coassembly of hBest1 with other channel subunits. (*A–F*) hBest1–mCherry coexpressed with either N- or C-terminal mEGFP-tagged: CNG channel (*A*), hBest1 (*B*), hBest2 (*C*), hBest3 (*D*), hBest4 (*E*), or mTMEM16A (*F*). Total number in all experiments combined of red-alone spots (red bars), green-alone spots (green bars), and spots containing both red and green fluorescence (orange bars), with percent of red + green indicated above orange bar. (*G*) Average percent colocalization for 5–10 optical patches for each coinjection. Error bars indicate SEM. hBests abbreviated as B1 to B4.

coexpressed with an untagged version of either hBest2, 3, 4, or mTMEM16A (Fig. 3 *B–E*). Comparing the frequency of observation of spots with four mEGFP–hBest1-bleaching steps, we found that untagged hBest1 drastically decreased the frequency of observation of four mEGFP–hBest1-bleaching steps (Student *t* test, $P < 0.01$), and untagged hBest2 modestly but significantly decreased this value (Student *t* test, $P < 0.05$); however, there was no effect of untagged hBest3, hBest4, or mTMEM16A (Fig. 3*F*). Together, the subunit counting and colocalization results suggest that hBest1 does not coassemble with the hBest3, hBest4, or mTMEM16A and coassemble only weakly with hBest2.

L_2 Domain Regulates the Heteromeric Assembly Among Bestrophins. Having seen that hBest channels preferentially assemble as homotetramers led us to wonder how this subunit-selective assembly is determined. To address this, we exploited the lack of interaction between hBest1 and hBest3 to ask if we could identify a domain whose transplantation from one to the other would transfer the ability to interact. We reasoned that the extensive similarity among hBests would allow domain swaps to be tolerated. We made chimeras between hBest1 and 3 and first confirmed that the swaps were tolerated by determining the stoichiometry of complexes formed by each chimera on its own. Each of the chimeras that we used formed homotetramers (Fig. S5), permitting us to proceed to determine the interaction between these chimeras and hBest1 or hBest3 using single-molecule colocalization.

We first found that a C-terminal–deleted hBest1 [hBest1Δ C-terminal domain (CT)] had a normal tetrameric stoichiometry (Fig. S5). Therefore, we focused our chimeras on a region from the N terminus up until amino acid 350 in the membrane-proximal C terminal. We began by transplanting from hBest1 the short-N-terminus cytoplasmic domain together with transmembrane domain S1 into hBest3 and termed this chimera "hBest3 (B1:S_1)." We observed only 5.9 ± 2.3% colocalization between hBest3 (B1:S_1) –mEGFP and hBest1–mCherry (Fig. 4*A*), significantly lower (Student *t* test, $P < 0.01$) than the colocalization rate observed for hBest1–hBest1 (26.2%, Fig. 2*B*) and closer to [not significantly different (Student *t* test, $P = 0.08$) from] the colocalization rate observed for hBest1–hBest3 (0.8 ± 1.2%, Fig. 2*D*). Next, we swapped either S_1L_1, $S_1L_1S_2$, or $S_1L_1S_2L_2$ of hBest3 with the ones from hBest1 (*S* = Transmembrane domain, *L* = Loop). We observed a similar low rate of colocalization between hBest3 (B1:S_1L_1) and hBest1 (3.1 ± 1.0%, Fig. 4*B*). We could not calculate the colocalization rate between hBest3 (B1:$S_1L_1S_2$) and hBest1 (Fig. 4*C* and Movie S1) due to the high mobility of the chimeric complexes, but their mobility in itself reflected a lack of interaction with hBest1–mCherry, which was immobile and whose immobile red spots were rarely associated with a green spot.

In contrast to the above results, when we examined the interaction between the chimera hBest3 (B1:$S_1L_1S_2L_2$) and hBest1 we found a high rate of colocalization (24.6 ± 4.7%, Fig. 4*D*), similar to the rate of hBest1–hBest1 colocalization (26.2%, Fig. 2*B*), suggesting that L_2 is involved in preferential self-assembly. We tested this by swapping only L_2 from hBest1 into hBest3 and observed a similar high rate of colocalization between hBest3 (B1:L_2) and hBest1 (32.4 ± 1.6%, Fig. 4*E*) as with hBest1–hBest1 (26.2%, Fig. 2*B*), confirming that the L_2 of hBest1 is sufficient for preferential self-assembly of hBest1 homotetramers. We obtained similar results for the reciprocal swap, with hBest1 (B3:L_2) having

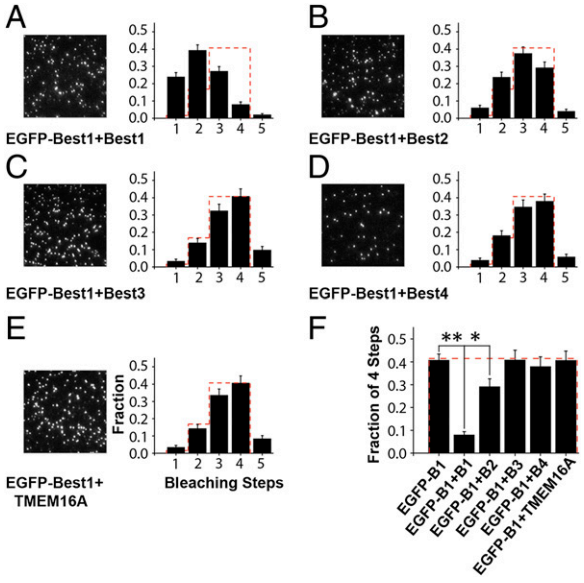

Fig. 3. Gauging coassembly of hBest1 with other CACC subunits by shifts in single-molecule subunit counts of mEGFP–hBest1. (*A–E*) Frequency distributions of single-molecule–photobleaching counts of mEGFP–hBest1 coexpressed with untagged hBest1 (number of optical patches $n = 6$) (*A*), hBest2 ($n = 7$) (*B*), hBest3 ($n = 5$) (*C*), hBest4 ($n = 4$) (*D*), or mTMEM16A ($n = 5$) (*E*), compared with the binomial distribution of tetramer with the probability that mEGFP is fluorescent = 0.8 (red dashed lines). (*F*) Fraction of spots with four bleaching steps when mEGFP–hBest1 is expressed alone (mEGFP–B1) or together with untagged hBestx (mEGFP–hBest1 + Bx) or untagged mTMEM16A (mEGFP–hBest1 + mTMEM16A).

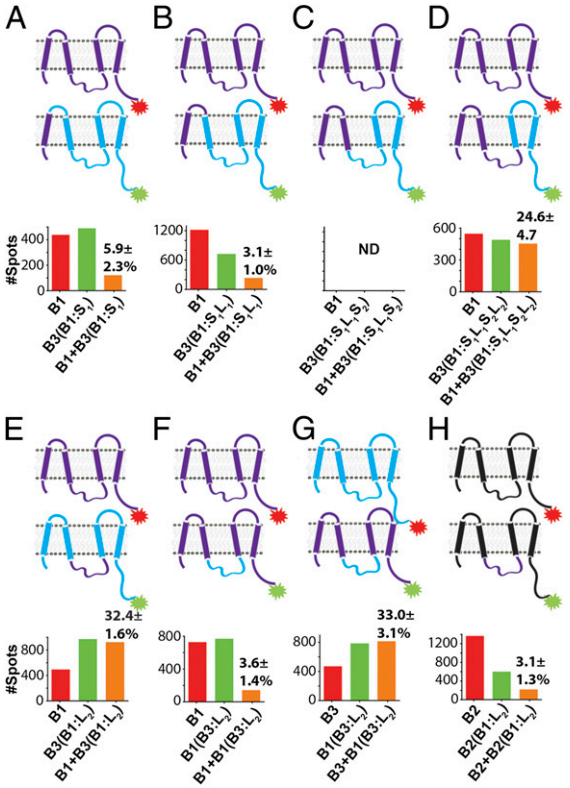

Fig. 4. Coassembly of hBests with hBest chimeras defines self-assembly determinant. (*A–F*) Colocalization of hBest1–mCherry (B1) with hBest3–mEGFP (B3) containing either the S_1 of B1 (*A*), the S_1 and L_1 of B1 (*B*), the S_1, L_1 and S_2 of B1 (*C*), the S_1 and L_1 and S_2 and L_2 of B1 (*D*), only the L_2 of B1 (*E*), or everything but the L_2 of B1 (*F*). (*G*) Colocalization of B3 with B1 containing the L_2 of B3. (*H*) Colocalization of B2 with B2 containing the L_2 of B1. Bar color code and percentage colocalization as in Fig. 2.

a high degree of colocalization with hBest3 (33.0 ± 3.1%, Fig. 4*G*), indicating that the sufficiency of L_2 for preferential self-assembly applies also to hBest3 homotetramers.

In complimentary experiments, we again asked whether L_2 is necessary for preferential self-assembly. A swap of the L_2 of hBest3 into hBest1, the chimera hBest1 (B3:L_2), had low colocalization with hBest1 (3.6 ± 1.4%, Fig. 4*F*). Similarly, hBest2 (B1:L_2) had a little colocalization with hBest2 (3.1 ± 1.3%, Fig. 4*H*). In summary, these results demonstrate that L_2 is both necessary and sufficient to confer specific homomeric assembly in hBest channels.

Coiled-Coil Domain in L_2 Is the Assembly Determinant. Having found that L_2 confers assembly specificity, we subdivided the domain to identify the minimal region required. Alignment of the L_2 domains of hBest1 and hBest3 revealed a 16-amino-acid-long segment, from 165 to 180, that is particularly divergent [Fig. 5*A*, variable region (Var)]. We also searched for possible protein association domains and found a predicted coiled-coil domain, using the Coils prediction software (41), at the C terminus end of L_2 in both hBest1 and hBest3 [Fig. 5*A*, coiled-coil domain (CC)]. Although these coiled-coil domains are similar in hBest1 and hBest3, they differ in the predicted number of heptads (three heptads predicted with a probability of ~0.7 in hBest1, but only with a probability of <0.1 in hBest3) (Fig. S6). We tested the ability of the variable and predicted coiled-coil regions to drive colocalization.

We observed a low rate of colocalization between hBest1 and hBest3 (B1:Var) (2.8 ± 1.1%, Fig. 5*B*). In contrast, we observed a high rate of colocalization between hBest1 and hBest3 (B1:CC) (33.4 ± 1.3%, Fig. 5*C*), comparable to the colocalization rate of hBest1–hBest1 (26.2%, Fig. 2*B*). This suggests that it is the coiled-coil domain of L_2 that allows the assembly between like subunits and prevents it between different members of the family.

Dual Role of Coiled-Coil Domain in Bestrophins. Several BMD-causing mutations have been mapped to the coiled-coil segment of hBest1, which has been called a mutational hot-spot (42). In light of the above results, this suggests that aberrant assembly can be a cause of pathology. To further examine the role of the coiled coil in channel function, we assessed the effects of protein swaps on ion conduction through the channel using the iodide-quenching assay as a measure of anion influx in HEK293T cells (43). hBest1 or hBest3 or one of the chimeras was coexpressed with P2Y receptors (whose activation by ATP liberates calcium from internal stores to activate hBest channels and allow iodide influx) along with an iodide-quenchable YFP sensor (YFP H148Q, I152L) (43). YFP fluorescence was measured during a 60-s baseline period in Ringer's solution (141 mM NaCl) and then for 120 s following a switch to 300 μM ATP in modified Ringer's solution (141 mM NaI). Consistent with previous studies, a ~30–50% decrease in fluorescence was observed in hBest1-expressing cells, whereas almost no quenching was observed in hBest3-expressing cells (Fig. 6*A*) (18, 26), because of the much smaller currents of hBest3 (1, 15). To confirm that the quenching was due to iodide conduction through hBest, we either introduced BMD-causing mutations (W93C or R218C) that are known to block ion conduction through hBest1 (7, 11) or deleted the Ca^{2+}-binding domain at the C terminus (Δ299–304) that is needed for the activation of hBest1 (24). As expected, we observed no ATP-triggered quenching in either of the mutants (Fig. 6*A*). To check that this absence of activity is actually due to the mutations and not due to their lack of expression, we expressed the mutants in oocytes and checked both their expression and stoichiometry. Both the mutants were found to have similar expression and stoichiometry compared with the wild-type hBest1 (Fig. S7). In addition, the robust expression of hBest3 in oocytes supported the interpretation that lack of quenching activity in hBest3 is due to smaller currents compared with hBest1, rather than to a lack of expression (Figs. 1 and 2). This

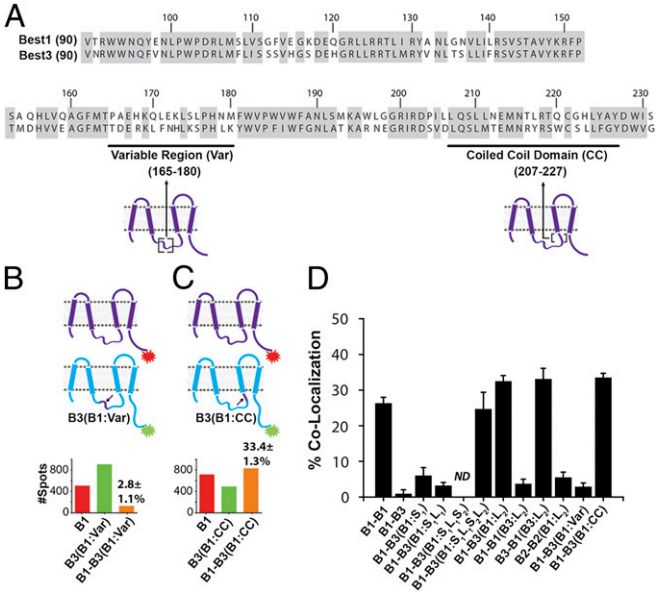

Fig. 5. Single-molecule colocalization identifies coiled-coil domain in L_2 as assembly determinant. (*A*) Protein sequence alignment of L_2 domains of hBest1 and hBest3 shows high conservation (gray highlights), except in Var and also identifies CC. (*B* and *C*) Colocalization of B1 with B3 containing only the Var of B1 (*B*) or with B3 containing only the CC of B1 (*C*). (*D*) Comparison of colocalization results obtained in Figs. 2, 4, and 5.

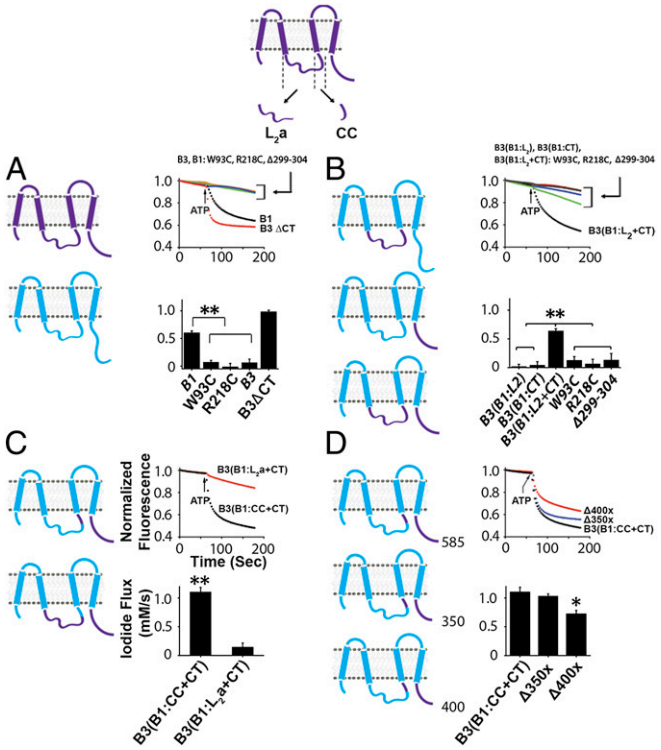

Fig. 6. Iodide-quenching assay determines the functional role of coiled-coil domain in hBests. Comparing iodide conduction, upon activation at ~60 s using ATP, through (*A*) hBest1 (black), two known hBest1-blocking mutants hBest1: W93C (green), hBest1:R218C (blue), Ca^{2+}-binding domain deletion (Δ299–304, purple), hBest3 (orange, known to have low conduction), and hBest3ΔCT (red, deletion known to increase conduction). (*B*) B1–B3 chimeras, B3(B1:L_2), B3(B1:CT) (no activity, red and gray, respectively), B3(B1:L_2 + CT) (black) (activity comparable to hBest1), hBest1-blocking mutants in L_2 + CT chimera, B3(B1:L_2 + CT):W93C (green), R218C (blue), and Ca^{2+}-binding domain deletion (Δ299–304, purple). (*C*) B1–B3 chimeras either having coiled coil from L_2, B3(B1:CC + CT) (black) or remainder of the L_2, B3(B1:L_2a + CT) (red). (*D*) B1–B3 chimeras either having full-length C terminus, B3(B1:CC + CT) (black) or truncated C terminus B3 (B1:CC + CTΔ350X) (blue) and B3(B1:CC + CTΔ400X) (red).

was further supported by our finding that, as shown before (16), deletion of the C terminus, containing autoinhibitory domain, of hBest3 (hBest3 Δ353–669) resulted in large ATP-triggered quenching (Fig. 6*A*).

We used the lack of activity in full-length hBest3 to ask whether L_2 would confer the channel activity of hBest1 into hBest3. We also examined the CT, which is poorly conserved (~14% identity between hBest1 and hBest3) and contains an autoinhibitory domain that blocks the current in hBest3 (16, 18). We observed no activity when only L_2 was transplanted from hBest1 into hBest3 [B3 (B1:L_2)], nor when only the CT was transplanted [B3 (B1:CT)] (Fig. 6*B*). However, when L_2 and the CT were transplanted together [B3 (B1:L_2 + CT)], quenching was comparable to that seen in hBest1 (Fig. 6*B*), suggesting a concerted function of these segments. To confirm that both L_2 and CT of hBest1 conferred hBest1-level activity onto hBest3, we again introduced either the BMD-causing mutations (W93C or R218C) into the hBest1 L_2 or deleted the Ca^{2+}-binding domain at the C terminus (Δ299–304) and transplanted each of these mutated versions of L_2 or CT into hBest3. Similar to the lack of activity of hBest1–W93C, R218C, and Δ299–304, we did not observe any significant activity in either of these L_2 or CT mutant chimeras (Fig. 6*B*), further supporting the interpretation that the activity level introduced into hBest3 is due to a transplantable function of the L_2 and CT of hBest1.

To more precisely map the portion of L_2 involved in conductance, we divided L_2 into two parts: the CC and the remainder of L_2 (L_2a) (Fig. 6, cartoon). Transplantation of L_2a in combination with the CT from hBest1 to hBest3 [B3 (B1:L_2a + CT)] did not confer hBest1-like activity, but such activity was observed upon transplantation of the CC in combination with the CT [B3 (B1:CC + CT)] (Fig. 6*C*), indicating that it is the coiled-coil region of L_2 that is crucial for its role in channel function.

Maintaining the coiled coil of hBest1 intact, we then determined the minimal region of the CT of hBest1 that is critical for function. We made two deletion mutants that truncated the protein at either amino acid 350 or 400, B3 (B1:CC + CTΔ350x) and B3 (B1:CC + CTΔ400x). Both swaps were found to be functional, but activity in Δ350x was significantly higher than Δ400x (Fig. 6*D*), perhaps due to the absence of the autoinhibitory domain that lies between amino acids 350 and 400 (16, 18). These results suggest that the Ca^{2+}-binding domain (amino acids 290–350) of hBest1 is sufficient to confer its gating properties, but only in conjunction with hBest1's own coiled-coil domain.

Patch clamp analysis yielded similar results from the chimeras (Fig. S8), confirming that both the coiled coil and C-terminal domains are required for activity in hBest1.

Discussion

Using single-molecule methods of subunit counting and colocalization exclusively on functional complexes at the plasma membrane of live cells, we find that, on its own, each hBest forms a homotetrameric channel. We found that hBest1 does not coassemble with the completely different CACC mTMEM16A. Strikingly, we find that, despite a high degree of conservation among hBests, hBest1 does not coassemble with hBest3 or hBest4. The only heteromeric assembly that we detected was with hBest2. This is consistent with earlier biochemical evidence (30), but the interaction seems to be too weak to produce a disease-inducing dominant negative effect in hBest1 point mutants. Also, the possibility of bestrophins forming heteromeric complexes in native tissues is limited due to their restricted distribution. The hBest1 mainly expresses in retina and RPE cells (1, 11, 44), whereas hBest2 and hBest4 express mostly in different cell types in colon (goblet cells and small intestine, respectively) (45, 46).

The absence of interaction between hBest1 and other members of the bestrophin family is striking given their high degree of identity. We found that the L_2 domain is both necessary and sufficient to determine specific self-assembly, and that it is the coiled-coil domain located at the C terminus of L_2 which is responsible. This coiled-coil domain has been identified as one of the four regions where mutations are associated with disease (42). Some of the mutations in the coiled-coil affect the surface expression of hBest1 in MDCKII cells (47), an expected outcome of disrupted assembly and a clear cause of pathology. However, at least one disease-causing mutation in the coiled coil (R218C) has no effect on the surface expression (47), suggesting that coiled-coil domain has other additional functions in the channel. We find that transplantation of the coiled-coil domain confers the large current of hBest1 on to hBest3 but only when the coiled coil is accompanied by cotransplantation of Ca^{2+}-binding domain of hBest1. This suggests that the coiled-coil domain also has a role in gating, perhaps coupling the Ca^{2+} binding at C-terminal domain of hBest1 with a rearrangement of S2, which earlier work identified as forming the pore (17, 19, 21).

According to the Milenkovic model (23), the coiled-coil domain resides inside the cell between S2 and S3, whereas according to the Tsunenari model (15), it lies outside the cell right before the reentrant loop. In either case, our findings suggest that a symmetric coiled-coil assembly made up of identical regions from each subunit is arrayed around the central axis of the pore and that conformational changes at the C terminus that are induced by calcium binding open the channel.

In summary, we find that hBest channels are tetramers with a strong preference for homomeric assembly, and we identify the domain that regulates this assembly and discover that this domain also plays a role in controlling the current.

Materials and Methods

Tagged human bestrophin1–4 and the chimeras were cloned in the pGEMHE vector and transcribed in vitro and injected into *Xenopus* oocytes. After 1–2 d of expression, oocytes were devitillinized and imaged using TIRFM as described in detail in *SI Materials and Methods*. Iodide imaging (43, 47) is described in *SI Materials and Methods*.

ACKNOWLEDGMENTS. We thank Jeremy Nathans and Lily Jan for providing the bestrophin and mTMEM16A clones, respectively; Hitomi Otsuki-Okada and Shivan Bonanno for their help with the cloning; Ryan Arant for his help with TIRFM; and members of the E.Y.I. laboratory for helpful discussion. This work was supported by National Institutes of Health Grants 2PN2EY018241 and R01 NS35549 (to E.Y.I.).

1. Hartzell HC, Qu Z, Yu K, Xiao Q, Chien LT (2008) Molecular physiology of bestrophins: Multifunctional membrane proteins linked to best disease and other retinopathies. *Physiol Rev* 88(2):639–672.
2. Park H, et al. (2009) Bestrophin-1 encodes for the Ca2+-activated anion channel in hippocampal astrocytes. *J Neurosci* 29(41):13063–13073.
3. Lee S, et al. (2010) Channel-mediated tonic GABA release from glia. *Science* 330(6005): 790–796.
4. Woo DH, et al. (2012) TREK-1 and Best1 channels mediate fast and slow glutamate release in astrocytes upon GPCR activation. *Cell* 151(1):25–40.
5. Han KS, et al. (2013) Channel-mediated astrocytic glutamate release via Bestrophin-1 targets synaptic NMDARs. *Mol Brain* 6:4.
6. Bakall B, et al. (1999) The mutation spectrum of the bestrophin protein—functional implications. *Hum Genet* 104(5):383–389.
7. Caldwell GM, et al. (1999) Bestrophin gene mutations in patients with Best vitelliform macular dystrophy. *Genomics* 58(1):98–101.
8. Hartzell C, et al. (2005) Looking chloride channels straight in the eye: Bestrophins, lipofuscinosis, and retinal degeneration. *Physiology (Bethesda)* 20:292–302.
9. Krämer F, Stöhr H, Weber BH (2004) Cloning and characterization of the murine Vmd2 RFP-TM gene family. *Cytogenet Genome Res* 105(1):107–114.
10. Marquardt A, et al. (1998) Mutations in a novel gene, VMD2, encoding a protein of unknown properties cause juvenile-onset vitelliform macular dystrophy (Best's disease). *Hum Mol Genet* 7(9):1517–1525.
11. Petrukhin K, et al. (1998) Identification of the gene responsible for Best macular dystrophy. *Nat Genet* 19(3):241–247.
12. Strauss O (2005) The retinal pigment epithelium in visual function. *Physiol Rev* 85(3): 845–881.
13. Davidson AE, et al. (2009) Missense mutations in a retinal pigment epithelium protein, bestrophin-1, cause retinitis pigmentosa. *Am J Hum Genet* 85(5):581–592.
14. Stöhr H, Marquardt A, Nanda I, Schmid M, Weber BH (2002) Three novel human VMD2-like genes are members of the evolutionary highly conserved RFP-TM family. *Eur J Hum Genet* 10(4):281–284.
15. Tsunenari T, et al. (2003) Structure-function analysis of the bestrophin family of anion channels. *J Biol Chem* 278(42):41114–41125.
16. Qu Z, Cui Y, Hartzell C (2006) A short motif in the C-terminus of mouse bestrophin 3 [corrected] inhibits its activation as a Cl channel. *FEBS Lett* 580(8):2141–2146.
17. Qu Z, Fischmeister R, Hartzell C (2004) Mouse bestrophin-2 is a bona fide Cl(-) channel: identification of a residue important in anion binding and conduction. *J Gen Physiol* 123(4):327–340.
18. Qu ZQ, Yu K, Cui YY, Ying C, Hartzell C (2007) Activation of bestrophin Cl- channels is regulated by C-terminal domains. *J Biol Chem* 282(24):17460–17467.
19. Qu Z, Hartzell C (2004) Determinants of anion permeation in the second transmembrane domain of the mouse bestrophin-2 chloride channel. *J Gen Physiol* 124(4): 371–382.
20. Qu Z, Wei RW, Mann W, Hartzell HC (2003) Two bestrophins cloned from Xenopus laevis oocytes express Ca(2+)-activated Cl(-) currents. *J Biol Chem* 278(49):49563–49572.
21. Qu Z, Chien LT, Cui Y, Hartzell HC (2006) The anion-selective pore of the bestrophins, a family of chloride channels associated with retinal degeneration. *J Neurosci* 26(20): 5411–5419.
22. Sun H, Tsunenari T, Yau KW, Nathans J (2002) The vitelliform macular dystrophy protein defines a new family of chloride channels. *Proc Natl Acad Sci USA* 99(6): 4008–4013.
23. Milenkovic VM, Rivera A, Horling F, Weber BH (2007) Insertion and topology of normal and mutant bestrophin-1 in the endoplasmic reticulum membrane. *J Biol Chem* 282(2):1313–1321.
24. Xiao Q, Prussia A, Yu K, Cui YY, Hartzell HC (2008) Regulation of bestrophin Cl channels by calcium: Role of the C terminus. *J Gen Physiol* 132(6):681–692.
25. Chien LT, Zhang ZR, Hartzell HC (2006) Single Cl- channels activated by Ca2+ in Drosophila S2 cells are mediated by bestrophins. *J Gen Physiol* 128(3):247–259.
26. Tsunenari T, Nathans J, Yau KW (2006) Ca2+-activated Cl- current from human bestrophin-4 in excised membrane patches. *J Gen Physiol* 127(6):749–754.
27. Stanton JB, Goldberg AF, Hoppe G, Marmorstein LY, Marmorstein AD (2006) Hydrodynamic properties of porcine bestrophin-1 in Triton X-100. *Biochim Biophys Acta* 1758(2):241–247.
28. Abuin L, et al. (2011) Functional architecture of olfactory ionotropic glutamate receptors. *Neuron* 69(1):44–60.
29. Durisic N, et al. (2012) Stoichiometry of the human glycine receptor revealed by direct subunit counting. *J Neurosci* 32(37):12915–12920.
30. McGuire H, Aurousseau MR, Bowie D, Blunck R (2012) Automating single subunit counting of membrane proteins in mammalian cells. *J Biol Chem* 287(43):35912–35921.
31. Reiner A, Arant RJ, Isacoff EY (2012) Assembly stoichiometry of the GluK2/GluK5 kainate receptor complex. *Cell Rep* 1(3):234–240.
32. Ulbrich MH, Isacoff EY (2007) Subunit counting in membrane-bound proteins. *Nat Methods* 4(4):319–321.
33. Ulbrich MH, Isacoff EY (2008) Rules of engagement for NMDA receptor subunits. *Proc Natl Acad Sci USA* 105(37):14163–14168.
34. Rosenthal R, et al. (2006) Expression of bestrophin-1, the product of the VMD2 gene, modulates voltage-dependent Ca2+ channels in retinal pigment epithelial cells. *FASEB J* 20(1):178–180.
35. Jain A, et al. (2011) Probing cellular protein complexes using single-molecule pull-down. *Nature* 473(7348):484–488.
36. Marchant D, et al. (2007) New VMD2 gene mutations identified in patients affected by Best vitelliform macular dystrophy. *J Med Genet* 44(3):e70.
37. Yu K, Cui Y, Hartzell HC (2006) The bestrophin mutation A243V, linked to adult-onset vitelliform macular dystrophy, impairs its chloride channel function. *Invest Ophthalmol Vis Sci* 47(11):4956–4961.
38. Yu K, Qu Z, Cui Y, Hartzell HC (2007) Chloride channel activity of bestrophin mutants associated with mild or late-onset macular degeneration. *Invest Ophthalmol Vis Sci* 48(10):4694–4705.
39. Marmorstein AD, et al. (2004) A model of best vitelliform macular dystrophy in rats. *Invest Ophthalmol Vis Sci* 45(10):3733–3739.
40. Marmorstein LY, et al. (2006) The light peak of the electroretinogram is dependent on voltage-gated calcium channels and antagonized by bestrophin (best-1). *J Gen Physiol* 127(5):577–589.
41. Lupas A, Van Dyke M, Stock J (1991) Predicting coiled coils from protein sequences. *Science* 252(5009):1162–1164.
42. White K, Marquardt A, Weber BH (2000) VMD2 mutations in vitelliform macular dystrophy (Best disease) and other maculopathies. *Hum Mutat* 15(4):301–308.
43. Galietta LJ, Haggie PM, Verkman AS (2001) Green fluorescent protein-based halide indicators with improved chloride and iodide affinities. *FEBS Lett* 499(3):220–224.
44. Mullins RF, Kuehn MH, Faidley EA, Syed NA, Stone EM (2007) Differential macular and peripheral expression of bestrophin in human eyes and its implication for best disease. *Invest Ophthalmol Vis Sci* 48(7):3372–3380.
45. Yu K, Lujan R, Marmorstein A, Gabriel S, Hartzell HC (2010) Bestrophin-2 mediates bicarbonate transport by goblet cells in mouse colon. *J Clin Invest* 120(5):1722–1735.
46. Ito G, et al. (2013) Lineage-specific expression of bestrophin-2 and bestrophin-4 in human intestinal epithelial cells. *PLoS ONE* 8(11):e79693.
47. Milenkovic VM, Röhrl E, Weber BH, Strauss O (2011) Disease-associated missense mutations in bestrophin-1 affect cellular trafficking and anion conductance. *J Cell Sci* 124(Pt 17):2988–2996.